CaxLa1xMn1yMyO3 (M = Mg, Ti, Fe or Cu) as Oxygen Carriers for Chemical-Looping with Oxygen Uncoupling (CLOU)

$Ca_xLa_{1-x}Mn_{1-y}M_yO_{3-\delta}$ (M = Mg, Ti, Cu or Fe) as Oxygen Carriers for Chemical-Looping with Oxygen Uncoupling (CLOU)

Mehdi Arjmand [a,*], *Ali Hedayati* [a], *Abdul-Majeed Azad* [b], *Henrik Leion* [a], *Magnus Rydén* [c], *Tobias Mattisson* [c]

[a] Department of Chemical and Biological Engineering, Division of Environmental Inorganic Chemistry, Chalmers University of Technology, SE-412 96 Göteborg, Sweden

[b] Department of Chemical Engineering, The University of Toledo, Toledo, OH 43606-3390 USA

[c] Department of Energy and Environment, Division of Energy Technology, Chalmers University of Technology, SE-412 96 Göteborg, Sweden

[*] To whom correspondence should be addressed. Telephone: +46-31-772-2822;

E-mail: arjmand@chalmers.se

Abstract

Perovskite materials of the type $Ca_xLa_{1-x}Mn_{1-y}M_yO_{3-\delta}$ (M = Mg, Ti, Fe or Cu) have been investigated as oxygen carriers for the chemical-looping with oxygen uncoupling (CLOU) process. The oxygen carrier particles were produced by mechanical homogenization of primary solids in a rotary evaporator followed by extrusion and calcination at 1300^{o}C for 6 h. The chemical-looping characteristics of the substituted perovskites developed in this work were evaluated in a laboratory-scale fluidized-bed reactor in the temperature range of 900−1000^{o}C during alternating reducing and oxidizing conditions. The oxygen carriers showed oxygen releasing behaviour (CLOU) in inert atmosphere between 900−1000^{o}C. In addition, their reactivity with methane was high, approaching complete gas yield for all of the materials at 950^{o}C, the exception being the Cu-doped perovskite which defluidized during reduction. The rates of oxygen release were also investigated using devolatilized wood char as solid fuel, and were found to be similar. The required solids inventory in the fuel reactor for the perovskite oxygen carriers is estimated to be 325 kg/MW_{th}. All of the formulations exhibited high rates of oxidation and high degree of stability with no particle fragmentation or agglomeration. The high reactivity and favourable oxygen uncoupling properties make these oxygen carriers promising candidates for the CLOU process.

Keywords: CO_2-capture; chemical-looping combustion (CLC); chemical-looping with oxygen uncoupling (CLOU); oxygen carrier; perovskite.

1. Introduction

As suggested by the intergovernmental panel on climate control (IPCC), a 50-85% reduction in total CO_2 emission by 2050 is necessary to limit the anticipated global temperature rise to 2°C.[1] A number of alternative technologies have been proposed to mitigate the rising levels of carbon dioxide in the atmosphere. Among these, carbon capture and storage (CCS) is considered promising.

Chemical-looping combustion (CLC) can give an essentially pure CO_2 stream from hydrocarbon combustion without any direct gas separation. In a CLC system, two reactors, a fuel reactor and an air reactor, are interconnected with an oxygen carrier circulating between these reactors.[2-4] When fuel and air are introduced into the reactors, the following overall reactions occur, i.e. reaction (1) in the fuel reactor, and reaction (2) in the air reactor,

$$(2n+m)Me_xO_y + C_nH_{2m} \rightarrow (2n+m)Me_xO_{y-1} + nCO_2 + mH_2O \quad (1)$$

$$2Me_xO_{y-1} + O_2 \rightarrow 2Me_xO_y \quad (2)$$

Here, Me_xO_y and Me_xO_{y-1} are the oxidized and reduced forms of an oxygen carrier. C_nH_{2m} is the fuel, which could be gas, liquid or solid. A schematic description of the process is shown in Figure 1. In case of complete conversion of the fuel, the exhaust stream from the fuel reactor consists of only CO_2 and H_2O, from which pure CO_2 could be obtained after condensation of water. The reduced oxygen carrier (Me_xO_{y-1}) is then transferred to the air reactor where it is re-oxidized by air making it ready for the next cycle. Thus in CLC, N_2 and CO_2 gases are never mixed. The oxidation reaction is always exothermic while the reduction reaction can be exothermic or endothermic depending on the fuel and the oxygen carrier.[5] However, the sum of the heat from reactions (1) and (2) is the same as for conventional combustion. Thus the CLC process does not entail any direct energy penalty for CO_2 separation. CLC has been successfully demonstrated in a number of units of sizes up to 120 kW.[6] Overviews of current achievements in CLC are given by Lyngfelt,[6, 7] Hossain and de Lasa[8] and Adanez et al.[9]

In the case of solid fuels, the char remaining after devolatilization is gasified in the presence of steam, producing CO and H_2, which then react with the oxygen carrier. An alternative to CLC for solid fuels using gasification of the char, is chemical-looping with oxygen uncoupling (CLOU),[10] in which the char reacts directly with gaseous oxygen released from the oxygen carrier. In

comparison to CLC where the reduction of oxygen carrier and oxidation of the gaseous fuel generally occurs in a single step, an additional step is needed in CLOU for the release of gaseous oxygen from the carrier prior to conversion of the fuel according to

$$Me_xO_y \rightarrow Me_xO_{y-2} + O_2 \quad (3)$$

This is followed by the normal combustion of the fuel via

$$C_nH_{2m} + (n + \frac{m}{2})O_2 \rightarrow nCO_2 + mH_2O \quad (4)$$

The reduced oxygen carrier is transferred to the air reactor for re-oxidation. The net heat of reaction for the CLOU process is the same as CLC and only the mechanism by which oxygen is accessed by the fuel differs. However, when using solid fuels like coal, the CLOU process avoids the slow gasification of the solid fuel needed to produce synthesis gas as a prerequisite for the reaction with the oxygen carrier.[10] The oxygen carrier in CLOU must be able to release O_2 and oxidize at temperatures suitable for the process, i.e. 800 to 1200^{o}C.

The most commonly proposed approach to realize CLC is to use inter-connected fluidized-bed reactors in a similar fashion as in a circulating fluidized-bed boiler (CFB),[2] the difference being that CLC will require an active oxygen carrier rather than inert sand as bed material. Conventional CFB boilers often operate at an air to fuel ratio of about 1.2, which means that the oxygen concentration at the outlet of the air reactor in a realistic CLC unit should be in the vicinity of 5%. Therefore, oxide systems with an equilibrium oxygen partial pressure lower than 5% at temperatures typical of the air reactor are desirable. Else higher air ratio will be required compared to conventional combustion, which would result in a slight efficiency penalty, if the aim is power generation via a conventional Clausius-Rankine cycle. The oxygen carrier should also be able to release sufficiently large amount of oxygen in the fuel reactor, at sufficiently high rate. These kinds of considerations limit the choice of oxygen carriers for the CLOU application.

An important aspect in the development of CLC and CLOU processes is the selection of oxygen carrier materials with adequate reactivity. Oxides of transition metals (Mn, Fe, Co, Ni and Cu), their mixtures, and a number of natural minerals (ores), industrial wastes and by-products have been used as oxygen carriers in CLC and CLOU.[6-9] High reactivity during oxidation and reduction over large number of cycles and the ability to fully convert the fuel are sought-after characteristics. In addition, thermal stability, mechanical strength, proper fluidization

characteristics and, resistance to attrition and agglomeration are also important. One way of achieving these is to mix the active phase (carrier oxide) with an inert support such as TiO_2, SiO_2, ZrO_2, Al_2O_3 or $MgAl_2O_4$ and/or heat-treat the oxygen carriers.[8]

ABO_3-type perovskites exhibit interesting properties by virtue of their oxygen non-stoichiometry.[11-17] This makes these materials interesting both for chemical-looping combustion (CLC) and chemical-looping with oxygen uncoupling (CLOU) applications, owing to their inherent ability to release significant amount of active oxygen through,

$$ABO_{(3-\delta)_{AR}} \leftrightarrow ABO_{(3-\delta)_{FR}} + \frac{1}{2}\left(\delta_{FR} - \delta_{AR}\right) O_2 \qquad (5)$$

The amount of oxygen released in the gas phase given by ½ ($\delta_{FR} - \delta_{AR}$), can be used to burn gaseous, liquid or solid fuel during the CLOU process. The term 'δ' gauges the degree of oxygen non-stoichiometry and 'AR' and 'FR' refer to the value of δ in the air and the fuel reactor, respectively. The oxygen non-stoichiometry of a perovskite material can be altered by changing parameters such as the ambient temperature or the O_2 partial pressure.[18] For example, in the oxidizing environment of the air reactor, δ_{AR} is determined by the partial pressure of oxygen at the outlet of the reactor, which is typically around 5%.[2] In the reducing environment of the fuel reactor, the partial pressure of O_2 is low. Therefore, at equilibrium δ_{FR} is larger than δ_{AR} which suggest release of gaseous oxygen.

One promising group of perovskite-type oxygen carrier materials belongs to the calcium manganate ($CaMnO_{3-\delta}$) family and its slightly altered variants which have shown excellent behaviour towards gaseous fuel combustion.[14, 15, 19] Assuming an O_2 partial pressure of 5% in the air reactor and a temperature of 950^{o}C in the air and the fuel reactor, the change in $3-\delta$ is approximately 0.04 for $CaMnO_{3-\delta}$,[20, 21] which corresponds to 0.5 wt. % of gaseous oxygen release from the carrier. Rydén et al.[15] examined $CaMn_{0.875}Ti_{0.125}O_{3-\delta}$ in a 300 W circulating fluidized-bed reactor and reported good fluidization behaviour, stable operation and steady O_2 release in inert atmosphere; complete conversion of CH_4 was also achieved. More recently, Källen et al.[19] investigated the performance of $CaMn_{0.9}Mg_{0.1}O_{3-\delta}$, in a 10 kW natural gas fired CLC unit. The results showed high rate of oxygen release and full conversion of natural gas, higher than NiO-based oxygen carrier in the same unit.[22, 23]

It has been suggested in the literature[20, 24] that undoped $CaMnO_{3-\delta}$ undergoes decomposition to $CaMn_2O_4$ and $Ca_2MnO_{4-\delta}$ with change in oxygen partial pressure in the ambient at medium to high temperatures. Although this decomposition is reported as reversible with respect to other applications, it has not been investigated in CLC. The present work reports on the performance of a series of A and B-site doped $CaMnO_{3-\delta}$-based oxygen carriers. Several formulations were synthesized with partial substitution of Ca with La at the A-site and that of Mn with Mg, Ti, Cu or Fe at the B-site. The substitution at both A- and B-site was restricted to 10 mol. %. The aim of doping at the A- and B-site was to investigate the changes in oxygen carrying capacity, performance, reactivity and stability of these carriers. The aliovalent doping in this class of compounds[25] is also a well-known strategy to induce oxygen non-stoichiometry.

2. Experimental

2.1 Preparation and fabrication of the oxygen carriers

The perovskite-based oxygen carrier particles investigated in this study and listed in Table 1, were manufactured as follows. $Ca(OH)_2$ (Alfa-Aesar, 95 wt. %) and Mn_2O_3 (Alfa-Aesar, 99 wt. %) powders with an average particle size ~46 μm (325 mesh) were mixed in appropriate weight ratio with or without La_2O_3 (Alfa-Aesar, 99.9 wt. %), MgO (Alfa-Aesar, 99 wt. %), TiO_2 (ACROS, 99 wt. %), Fe_2O_3 (Alfa-Aesar, 99 wt.%) and CuO (Alfa-Aesar, 97 wt. %) to make 170 g batches of the final product in each case.

Each mixed batch was transferred to a 1-liter pear-shaped distillation flask with 400 g of water, which was placed in a programmable 20-liter water bath. The aqueous slurry was thoroughly mixed and homogenized in a rotary evaporator (Büchi R-110) unit that was interfaced with a vacuum pump (Büchi V-710), a programmable vacuum controller (Büchi V-850) and a recirculating chiller (Büchi F-105). The rotary evaporator was operated by the 20/40/60 rule, 20°C being the cooling water temperature in the chiller, 40°C the boiling temperature of the water used as solvent at the reduced pressure, and 60°C being the bath temperature. The rotary evaporator operation was initiated at relatively low vacuum level (600 mm of Hg), and as the evaporation continued, the vacuum level was increased gradually (850 mm of Hg). This pressure modulation varied from system to system. The duration of the evaporation was about 2 h for each batch, which ensured thorough mixing, and uniform homogenization of the powders. When about two-thirds of the water had been removed by evaporation, it resulted in concentrated and viscous

but smooth flowing slurry. The slurry was poured into a shallow pan (Pyrex) and dried at 150°C in an air oven overnight. The dried soft cakey mass was then crushed and ground to a homogenous powder for each batch.

The resulting powders were used for extrusion. In each case, 170 g of the powder was weighed and mixed manually in a wide-mouthed plastic container with 10 g of polyvinyl alcohol (Alfa-Aesar) with average molecular weight ~25000 as a binder, 2 g of soluble $(C_6H_{10}O_5)_n$ starch (Merck) as an auxiliary binder, and 2 g of LAROSTAT 519 (PPG Industries) which is a quaternary ammonium salt, functioning as anti-static agent to increase the flux properties of the mixture. A mixture containing 4 g of 1 M ammonium hydroxide as peptizing agent and 78-90 g of water was added slowly to the solid ingredients with constant and quick stir-mixing. The amount of water varied from formulation to formulation depending up on the nature of B-site dopant. The somewhat wet mixture was then transferred to a food processor for mixing and homogenization. The ingredients were mixed mechanically, with intermittent stirring with plastic spatula, until pliant and flexible dough of desired plasticity suitable for extrusion was obtained.

The dough was transferred to a hand-held single-screw extruder and squeezed to form individual strands. This process helped in avoiding the fine dust formation when the powder was directly transferred to the food processor for mixing and also yielded the most optimum strands. This procedure proved to be optimal in producing the dough for reproducible extrusion. The strands were collected on a stainless steel sheet and dried in an air oven at 200-220°C overnight. The dried extrudates were transferred to high-density alumina crucibles and calcined in air for 6 h at 1300°C in a programmable muffle furnace, using the temperature-time profile shown in Figure 2. The calcined extrudates were sieved through stainless steel screens to yield particles in the range of 125-250 μm.

2.2 Characterization of the oxygen carriers

Crystalline phase determination of the oxygen carriers was carried out using powder X-ray diffraction (Bruker AXS, D8 Advanced) with $CuK_{\alpha 1}$ radiation. The bulk density was measured for particles in the size range of 125-180 μm using a graduated cylinder. The Brunauer-Emmett-Teller (BET) specific surface area was measured by N_2-adsorption (Micromeritics, TriStar 3000). The particle size distribution (PSD) was determined using a light microscope (Nikon, SMZ800) and ImageJ software[26] which measured the area of an ellipse fitted to a large number of particles.

The crushing strength (force needed to fracture a single particle) was measured using a digital force gauge (Shimpo, FGN-5) for particles in the size range of 180-250 μm. An average of 30 measurements was taken as the representative crushing strength. The morphology of the particles was examined with an environmental scanning electron microscope (ESEM) fitted with a field emission gun (FEI, Quanta 200).

The attrition rate of the particles (sized 125-180 μm) was measured using a customized jet cup rig,[27] which simulates the effects of grid jet attrition and cyclone attrition in a circulating fluidized-bed combustor. Six measurements, in the interval of 10 min. were made for the particles. Approximately, 5 g of a sample was placed inside the cup and the apparatus was assembled. Air at 10 l/min. was introduced at the nozzle, which corresponds to an air jet velocity of approximately 94 m/s. To avoid static electricity, which otherwise would cause particles to adhere to the inner walls of the apparatus, the air was humidified by bubbling air through a column of water. These experiments were carried out at room temperature and near atmospheric pressure.

In order to assess the oxygen capacity (R_O) of the investigated formulations for CLOU, reduction-oxidation cycles were carried out in a thermogravimetric analyser (Netzsch, STA 409 PC *Luxx*). Approximately 25 mg of a sample (125-180 μm) was placed inside the crucible and the experiment was initiated by heating in an oxidizing environment (20.8% O_2), with an inlet flow rate of 50 mL_N/min. The heating rate was a linear ramp of 40^oC/min and after reaching 950^oC, the temperature was maintained constant for 30 min. The sample was then exposed to a stream of high purity N_2 for 30 min. with an inlet flow rate of 50 mL_N/min, while keeping the temperature constant. These reduction-oxidation cycles were repeated three times. Prior to this, the thermobalance was calibrated with an empty Al_2O_3 crucible under identical experimental conditions.

2.3 Experimental setup and procedure in fluidized-bed reactor

Experiments for examining oxygen uncoupling and reactivity aspects were carried out in a quartz fluidized-bed reactor, 870 mm high and 22 mm in inner diameter. The scheme of the experimental setup used in this investigation is shown in Figure 3. A porous quartz plate was placed at a height of 370 mm from the bottom and the reactor temperature was measured with chromel-alumel (type K) thermocouples sheathed in inconel-600 located about 5 mm below and

25 mm above the plate. Pressure transducers (Honeywell) were used to measure the pressure drop over the bed of particles and the quartz plate at a frequency of 20 Hz. The pressure drop over the quartz plate is approximately constant for constant flows. Thus by measuring the fluctuations in the pressure drop, it is possible to determine if the particles were fluidized or not, i.e. a defluidization would be noted from a decrease in pressure fluctuations. The exit gas stream from the reactor was led into a condenser to remove water, which is generated during oxidation of the fuel. The composition of the dry gas was measured by a Rosemount NGA-2000 analyzer which measured the concentration (sensitivity of 0.001%) of O_2 through a paramagnetic channel, CO_2, CO and CH_4 through infrared channels and H_2 through difference in thermal conductivity of H_2 and N_2.

15 g of the sample was placed on the porous plate and the reactor was heated to 900°C in 5% O_2-balance N_2 mixture, in order to oxidize the oxygen carrier fully, prior to experiments. The use of 5% O_2 mixture was aimed at being close to the expected condition at the air reactor's outlet in a realistic CLC unit. Henceforth, the term cycle will be used to describe a redox cycle involving reduction of the oxygen-carrier sample in inert gas or fuel, followed by oxidation with the aforementioned 5% O_2 mixture. A set of three inert gas (N_2) cycles were carried out at 900 and 1000°C for 360 s, before and after fuel cycles for all samples to investigate the oxygen release. Methane and synthesis gas (50% CO-50% H_2) were used as fuel for 20 and 80 s, respectively, during the reduction periods at 950°C. Nitrogen was used as an inert purge for 60 s in between oxidation and reduction. Each cycle was repeated three times to establish reproducibility of the performance. Flow rates of 450, 600 and 900 mL_N/min were used during reduction, inert and oxidation, respectively. These flow rates were chosen to achieve a value of the superficial gas velocity, U, in the reactor approximately 4 to 7, 7 to 13 and 11 to 20 times higher than the calculated minimum fluidization gas velocity, U_{mf}, of the oxygen carrier particles during reduction (with methane), inert and oxidation periods, respectively. The minimum fluidization velocity, U_{mf}, was calculated by using the correlation given by Kunii and Levenspiel.[28]

In order to obtain the rate of oxygen release from the carrier as per reaction (5), it needs to be exposed to an oxygen-deficient environment at a suitable temperature. However, when nitrogen is used to simulate such a condition, reaction (5) may approach a condition close to that corresponding to equilibrium oxygen concentration, thus releasing oxygen at a limited rate. This rate could be slower than the actual rate in a real process, in which the released oxygen is

consumed by a fuel. Therefore, such an experimental approach would not readily yield the relevant rate of oxygen release since this rate is likely hindered by the oxygen released surrounding the particles. In the present case, the rate of oxygen release was obtained by using devolatilized wood char (Skogens Kol AB) as fuel. The oxygen carrier was fluidized with N_2, thus eliminating the likelihood of side reactions via gasification. In this way, the released oxygen reacts directly with the char, keeping the ambient O_2 concentration low. Since the wood char is free of volatiles, the rate of char combustion should be strictly correlated to the rate of oxygen release from the oxygen carrier. This is similar to the method used in a previous investigation, where the rate of oxygen release from $MgAl_2O_4$-supported CuO oxygen carrier was obtained.[29] The wood char was crushed and sieved to the same size range as that of the carrier particles, i.e. 125-180 μm. The devolatilization was carried out in a thermogravimetric analyzer (Leco, 701) at 920^{o}C for 3 h in N_2 stream. Table 2 shows the analysis of fresh and devolatilized wood char. The high carbon and low hydrogen and ash content helps in determining the rate of oxygen release conveniently and accurately, by measuring the concentration of CO_2 and O_2 near the reactor exit.

For the oxygen release rate measurement, the amount of oxygen carrier in the bed was decreased by mixing with an inert material. 6 g of the carrier was mixed with 9 g of quartz (Sigma-Aldrich), sieved to the same particle size range. 0.1 g of the devolatilized wood char was introduced from the top of the reactor, after approximately 1 min. from the start of the reduction (inert) period. This was to eliminate the possibility of fuel combustion in oxygen left from the preceding oxidation period. This also allowed for the conditions in the reactor to reach close to equilibrium conditions with regard to oxygen concentration. The fuel was introduced together with a sweep flow of 300 mL_N/min N_2 in order to ensure that all fuel reached the reaction zone in the reactor. The end of reduction was indicated by the decreasing concentration of CO_2 concentration at the outlet, after which, oxidation in 5% O_2 was carried out. The redox cycles were carried out at 950^{o}C, repeating each cycle three times. An inlet flow rate of 900 mL_N/min was used during both oxidation and reduction periods. This flow rate gave superficial gas velocity U, approximately 11 to 20 times higher than the calculated minimum fluidization gas velocity, U_{mf},[28] of the oxygen carrier particles during the reduction and oxidation periods.

2.4 Data analysis

The oxygen carrying capacity (R_O) of the investigated carriers for CLOU is defined as the mass change of oxygen in the samples as follows:

$$R_O = \frac{m_{ox} - m_{red}}{m_{ox}} \tag{6}$$

where m_{red} and m_{ox} are the mass of the oxygen carrier in oxidized and reduced states, respectively.

The reactivity of the oxygen carriers in the fluidized-bed apparatus is quantified in terms of gas yield or conversion efficiency, γ, and is defined as the fraction of fully oxidized fuel divided by the carbon containing gases in the outlet stream. For methane as fuel, the gas yield, γ_{CH_4} is calculated as

$$\gamma_{CH_4} = \frac{y_{CO_2}}{y_{CO_2} + y_{CH_4} + y_{CO}} \tag{7}$$

Here, y_i denotes the concentration (vol. %) of the respective gas, obtained from the gas analyzer. For 50% CO in H_2 as fuel, the gas yield, γ_{CO}, is similarly defined as in eq. (7) but with $y_{CH_4} = 0$.

The mass-based conversion of the oxygen carrier, ω, is defined as:

$$\omega = \frac{m}{m_{ox}} \tag{8}$$

where m is the actual mass of the oxygen carrier.

Using methane as fuel, eq. (9) is employed for calculating ω as a function of time during the reduction period from the measured concentrations of various gaseous species:

$$\omega_i = \omega_{i-1} - \int_{t_0}^{t_1} \frac{\dot{n}_{out} M_O}{m_{ox}} \left(4y_{CO_2} + 3y_{CO} + 2y_{O_2} - y_{H_2}\right) dt \tag{9}$$

Where ω_i is the instantaneous mass-based conversion at time i, ω_{i-1} the mass-based conversion in the preceding instant, t_0 and t_1 the initial and final time of measurement, M_O the molar mass of oxygen, and $\dot{n}_{out}$ the molar flow rate of dry gas at the reactor outlet.

In case of 50% CO in H_2 as fuel, eq. (10) is used for calculation of ω,

$$\omega_i = \omega_{i-1} - \int_{t_0}^{t_1} \frac{\dot{n}_{out} M_O}{m_{ox}} \left(2y_{CO_2} + y_{CO} + 2y_{O_2} - y_{H_2}\right) dt \quad (10)$$

The mass-based conversion of the oxygen carrier, ω, during reduction with the devolatilized wood char was similarly defined according to eq. (11), however, taking into account the concentrations of only CO_2 and O_2,

$$\omega_i = \omega_{i-1} - \int_{t_0}^{t_1} \frac{\dot{n}_{out} M_O}{m_{ox}} \left(2y_{CO_2} + 2y_{O_2}\right) dt \quad (11)$$

3. Results

3.1 Oxygen uncoupling of the carriers

Figure 4 shows the oxygen release profiles during inert gas purge at 900°C for all the samples. Evidently each perovskite formulation exhibited oxygen uncoupling behaviour. The oxygen release trend in each of the six carriers is quite similar, indicated by a steady decline in the amount of released oxygen as a function of time. This is typical for the perovskite-type of materials, where two mechanisms are believed to be dominant: (a) the oxygen non-stoichiometry is an artefact of defect chemistry and (b) the release or uptake of oxygen is a function of oxygen partial pressure in the ambient, according to reaction (5). Since the parent compound ($CaMnO_{3-\delta}$, CM) has the highest oxygen content (smallest δ), the amount of oxygen release via uncoupling in the inert environment is the highest. Doping at the A-site alone (CLM) affects the magnitude of oxygen non-stoichiometry, which is reflected in its oxygen profile which is lower than that of CM. In the light of the above rationale, the amount of oxygen releases is even lower for doubly-doped formulations, with CLMT showing the smallest release. Interestingly, the behaviour of Cu-doped material (CLMC) was different from others in the same series. For instance, while it followed similar trend up to ~120 s, the amount of released oxygen became almost non-variant at about 1% for the remainder of the inert period. In fact, during the latter part of the inert period, CLMC released the highest amount of oxygen among all the doped perovskites investigated here. The CLOU experiments were carried out over a number of cycles to ascertain the reproducibility of the observed behaviour; there was little difference from cycle to cycle, indicating that these oxygen carriers were stable and were not deactivated during successive cycles.

3.2 Reactivity of the Oxygen Carriers

The reactivity experiments were performed with methane as fuel at 950°C using 15 g of particles in the bed. A typical concentration profile during the reduction period for CLMF is shown in Figure 5. To begin with, the carrier is oxidized in 5% O_2 but, when the oxidizing stream is replaced with pure nitrogen (inert), the oxygen concentration decreases steadily in the same way as seen in Figure 4 for the oxygen uncoupling tests. Upon addition of fuel, CO_2 is evolved as a result of methane conversion; no CO or CH_4 was detected. At the same time, oxygen concentration decreases to zero. After complete conversion of fuel in the early part of reduction, some methane could be detected in the reactor outlet. Thus, it is likely that the reduction of perovskite carrier by methane consists of a combination of two reactions: (1) direct reaction of methane with the solid particles (via CLC) and (2) indirect reaction of methane with the gaseous oxygen released from the carrier (via CLOU). This aspect is discussed in more detail in Section 3.3. Also shown in Figure 5 is the oxygen concentration profile during oxidation (in 5% O_2) at 950°C, following the reduction period. Initially, the depleted oxygen carrier consumes all oxygen in the inlet stream. After about 1 min., oxygen breaks through and increases steadily, finally approaching and levelling off at the inlet concentration (5%). The fact that no oxygen is seen during the initial stages of oxidation suggests that the carrier had seen high degree of reduction. Consequently, the oxygen partial pressure is rather low at that point, which explains why most of the oxygen was consumed in the early part of the oxidation period by the oxygen-depleted carrier. Table 3 shows the oxygen concentrations after 360 s of inert gas purges at 900°C and 1000°C, before and after the fuel cycles. As can be readily seen, there is no or very little loss in oxygen release behaviour over the fuel cycles even at 1000°C, confirming that these oxygen carriers are quite stable even when severely reduced with the fuel. The copper-doped formulation (CLMC) defluidized at 950°C during the reduction period, thus no relevant data could be obtained for CLMC. However, when the samples were retrieved from the reactor, no agglomeration or channelling in the bed could be observed. For CLMC in particular, the flow rate during reduction was increased and the reduction time decreased; still defluidization could not be avoided.

Figure 6 shows the gas yield, γ_{CH_4}, as a function of the mass-based degree of conversion, ω, for the third methane period for all the carriers investigated here (except CLMC, which defluidized

during reduction). Clearly, all materials showed high gas yield which was more than 88% during the entire reducing period.

The reactivity of the carriers was also investigated with synthesis gas (50% CO in H_2) and the corresponding gas yield, γ_{CO}, with respect to CO was calculated. There was complete gas yield (100%) at 950°C for all of the formulations, with the solid conversion reaching 0.98, i.e. change in ω of 2%. The results of methane and synthesis gas as well as solid conversion compare rather well with those reported for $CaMn_{0.875}Ti_{0.125}O_{3-\delta}$.[14]

3.3 Rate of oxygen release from the carriers

In order to obtain a rate of oxygen release from the carriers via the CLOU mechanism where the overall rate of reaction is not governed by the equilibrium partial pressure of oxygen, all of the released oxygen should preferably be seen in the form of CO_2. At this point, the rate of $ABO_{3-\delta_{AR}}$ decomposition is least hindered by the presence of oxygen around the particles. Taking only the carbon content of the devolatilized wood char into account (Table 2), it was estimated that 0.1 g of the fuel should be more than sufficient for the reduction of 6 g of the oxygen carrier, for obtaining the rate of oxygen release from the carrier in the CLOU region. In this context, it can be assumed that all of the released oxygen would be consumed by the solid fuel, which would be detected as CO_2 by the analyzer.

The oxygen concentration profile during CLOU process for the CM sample at 950^{o}C is shown in Figure 7 for illustrative purpose. Due to the dilution caused by the sweeping gas, the in-reactor concentrations obtained from mass-balance over the reactor system are also included. The O_2 concentration profile during the 60 s inert period prior to the introduction of devolatilized wood char is very similar to that in the inert background, as seen from Figure 4. Furthermore, the absence of peaks due to CH_4, CO or H_2 confirmed that the wood char was free of volatiles and that the char reacted with the gaseous oxygen alone from the carrier. As a result of this, the oxygen partial pressure drops rapidly to near zero within a short period. This indicates that the oxygen release step is the overall rate limiting reaction and, therefore, the rate of oxygen release is the overall reaction rate. Here, the rate of oxygen release from the carriers is at a maximum at the given conditions, as the driving force for the reverse reaction is removed entirely. As there was an excess of carbon introduced to the bed, there was a burn-off of the remaining carbon during the subsequent oxidation period of every cycle resulting in formation of CO_2. The amount

of carbon converted during reduction was approximately 0.01 g and was almost constant in every cycle. Although solid-solid reaction between fuel and oxygen carrier particles is possible,[30] it is very unlikely to affect the experimental results since such reactions are not fast enough under the fluidized-bed reactor conditions employed. Thus, the rates shown in Figure 7 are representative of the rate of gaseous oxygen release from the carrier.

Figure 8 shows the derivative of the mass-based conversion $\left(\frac{d\omega}{dt}\right)$, as a function of mass-based conversion, ω, of various oxygen carriers at 950°C. The non-variant regime of the plot during the first 60 s span (before the introduction of fuel) is indicative of the approach and establishment of near equilibrium conditions in the reactor with respect to oxygen concentration. Clearly, the reduction of the oxygen carrier is slow during this period. When fuel is added, the gaseous oxygen in the vicinity of the carrier is consumed almost instantly. This would create a rather large chemical potential gradient, thus making the perovskite carriers release additional oxygen at the highest possible rate. This is supported by the sharp spike in the curves. Interestingly, CM and CLMT exhibited, respectively, the highest and the lowest rate of oxygen release. It is also worth mentioning that the maximum oxygen release rate (~0.0002−0.0003 1/s) here is about 20 times lower than that for 1 g of $MgAl_2O_4$-supported CuO (0.005 1/s) at 900°C.[29] This is expected since it is well established that the rate of oxygen release for the CuO-based carriers is much higher. Using a methodology used previously,[29] the required solid inventory of perovskites in a fuel reactor operating at 950°C was estimated to be 325 kg/MW_{th}, assuming carbon as fuel with a lower heating value (LHV) of 32.8 MJ/kg, an average R_o of 0.5% for the oxygen carriers and solids circulation rate of 16 kg/s.MW_{th}.

Figure 9 shows the variation of mass-based conversion, ω, with time for the reduction with methane and 0.1 g of devolatilized wood char. The ω profiles for the conversion of devolatilized wood char are representative of the reaction pathway for the char with gaseous oxygen released from the carrier via CLOU, whereas in the case of methane, it is a combination of direct reaction of methane with the solid carrier via CLC and with gaseous oxygen via CLOU. As can be seen, the amount of oxygen released by the CLOU mechanism is smaller than that available for reaction with gaseous fuels such as CH_4 via the CLC process. This suggests that perovskite-based carriers are likely to react via a combination of CLC and CLOU mechanisms both; the relative

extent of each of these would depend upon the degree of conversion of oxygen carrier in the reactor.

3.4 Attributes of the oxygen carriers after redox cycle

Figure 10 shows the oxygen capacity of the materials for CLOU after the reactivity tests by thermogravimetric analyzer, when cycled between air (20.8% O_2) and high purity N_2. The slightly higher capacities (compared to those in Figure 8 and 9) are expected due to the higher oxygen partial pressure (20.8% vs. 5%) used here. As can be seen, R_O varies between 0.37 (for CLMT) to 0.76 (for CM). The R_O for CM corresponds well with the expected change in 3−δ reported by Bakken et al.[20] and Leonidova et al.[21] Doping at the A- and the B-sites both evidently resulted in decrease in oxygen capacity. Rørmark et al.[24] have also reported a lower oxygen transfer capacity for $Ca_{0.9}La_{0.1}MnO_{3-\delta}$ compared to $CaMnO_{3-\delta}$.

The oxygen carrier particles were also investigated subsequent to the reactivity tests to understand the mechanistic and structural changes that these materials undergo during the redox processes. The XRD analyses of fresh as well as used samples for CM, CLM and CLMT are shown in Figure 11. In the case of the used samples, the reactivity cycles where ended in N_2, synthesis gas and oxidation (5% O_2) streams at 950^{o}C, respectively. A thorough analysis of the XRD signatures is made difficult due to the superimposition of several diffraction peaks. Also, in the case of B-site doped composition, the software suggests $Ca_{0.85}La_{0.15}MnO_3$ or $Ca_{0.9}La_{0.1}Mn_{0.8}Ti_{0.2}O_3$ compounds, even though the doping in the either case was only 10 mole%. Other oxygen-deficient perovskite structures, however, could be identified in terms of their distinct peaks. In all cases, oxidation of the reduced samples restored the composition similar to that of the fresh oxygen carrier. Minor amount of the $CaMn_2O_4$ spinel in the oxidized and reduced samples were also detected. In the light of XRD patterns, the phase evolution could be classified into two categories, corresponding to two different behaviours predominantly in the synthesis gas environment: (1) The $CaMnO_{3-\delta}$ (CM) and A-site doped $Ca_{0.9}La_{0.1}MnO_{3-\delta}$ (CLM) samples were reduced by synthesis gas, forming $CaMnO_2$ phase (characterized by peak splitting at $2\theta = 34.5^o$ and 60.5^o). The regeneration of the parent perovskite CM upon oxidation (Figure 11; bottom) is in accordance with several studies.[20, 24, 31, 32] Formation of $CaMnO_2$ is visually verified by the characteristic olive-green colour[31, 33] of the particles after the reduction of CM by synthesis gas. Thus, in the case of $CaMnO_{3-\delta}$ (CM) and $Ca_{0.9}La_{0.1}MnO_{3-\delta}$ (CLM), Mn changes

from Mn^{4+} to Mn^{2+} as they transform into $CaMnO_2$ upon reduction at high temperatures. (2) In the case of A- and B-site doped particles (CLMT, CLMF, CLMM), the XRD patterns looked very similar to one other in all cases without any evidence of $CaMnO_2$ formation after reduction by synthesis gas. This suggests that the doubly-doped compounds are less prone to phase separation as opposed to their undoped and the singly-doped analogues.

Table 4 shows the bulk density and BET specific surface area of the used samples. Interestingly, the BET specific surface area did not change considerably; small changes could be due to measurement uncertainties. However, the bulk density decreased substantially, which could partly be due to the fact that the oxygen content in these samples is somewhat lower, as these were reoxidized in 5% O_2, in contrast to their fresh counterparts which were heat-treated in air (21% O_2).

The particle size distribution (PSD) of the oxygen carriers before and after reactivity test is shown in Figure 12. In the case of CLMT, the presence of fine particles in the fresh samples is noticeable. These fine particles were most likely entrained from the reactor during the reactivity test. The PSD for the rest of the oxygen carriers is quite similar and close, before and after the reactivity tests.

The perovskite-based oxygen carriers also showed reasonable mechanical strength, as indicated by the crushing strength measured prior to the reactivity tests. All particles (in the size range of 180-250 μm) had a crushing strength higher than 1 N (Table 1). It should be noted that the crushing strength might not correlate linearly with attrition and fragmentation behaviour in a real CLC system. With the exception of the Cu-doped material, defluidization did not occur for any of the particles during reactivity evaluation; no dust formation was observed either. However, given that the total number of cycles and the gas velocities employed in this work are rather low, further long-term tests will be needed in order to confirm the mechanical stability of these materials.

Figure 13 shows the rate of attrition of the used oxygen carriers during testing in a jet-cup attrition rig for 1 h. It can be noted that up to approximately 30 min., the rate of attrition is quite high. This is likely due to erosion of sharp edges, which are then entrained in the early stage of the test. Here, the attrition index, A_i, is defined as the slope of the attrition in the last 30 minutes of the test period, where stable values of attrition rates are achieved. Although the presented rates

are still not sufficiently low for a realistic CLC unit, they are within the range of other oxygen carriers tested in the same rig with satisfactory operation during hot experiments.[27] It is however, clear that for use in a full scale plant, the mechanical resistance of these particles would need to be increased, e.g. by changing or optimizing the manufacturing technique.

The ESEM images of the fresh and used CLM oxygen carrier are shown in Figure 14 (a-b), as an example. The surface morphology of the used particles did not change in any noticeable way. Moreover, the porosity of the particles did not seem to be affected by the redox testing compared to the fresh samples.

4. Conclusion

A series of novel doped perovskite-type oxygen carrier particles were synthesized by extrusion technique and investigated with respect to their oxygen uncoupling properties (CLOU) and, reactivity with methane, synthesis gas and devolatilized wood char. It is shown that doping at A- and B-sites decreases the oxygen transfer capacities of the various investigated formulations. With the exception of Cu-doped material which defluidized, almost complete methane gas yield was obtained at 950°C. With synthesis gas, complete gas yield was obtained for all materials at the same temperature. Neither particle fragmentation nor agglomeration was noticed during the experiments. All particles exhibited CLOU behaviour, which is an advantage especially with respect to solid fuel conversion. The reactivity tests showed that this class of oxygen carriers would react both via CLC and CLOU, in the fuel reactor. Their rate of oxygen release in the CLOU regime was investigated using devolatilized wood char as fuel and the required solids inventory in the fuel reactor using these materials is estimated to be 325 kg/MW_{th}. The high reactivity and favourable oxygen uncoupling properties make these oxygen carriers interesting for the CLOU process.

Acknowledgments

The authors wish to acknowledge Chalmers University of Technology via the Energy Area of Advance and European Research Council (Seventh Framework Programme under agreement No. 291235) for the financial support of this work. This study was also partly funded by Magnus Bergvalls Stiftelse. One of the authors (AMA) wishes to thank the United States Council for International Exchange of Scholars, for the Fulbright Distinguished Chair Award in Alternative Energy Technology at Chalmers University of Technology. Special thanks also go to Dr.

Christopher S. Knee (Chalmers University of Technology) for assisting with measurement with thermogravimetric analyzer.

References

(1) Pachauri, R. K.; Reisinger, A. *Fourth Assesment Report: Climate Change (Synthesis Report)*; Intergovernmental Panel on Climate Change: Geneva, 2007.
(2) Lyngfelt, A.; Leckner, B.; Mattisson, T. A fluidized-bed combustion process with inherent CO_2 separation; application of chemical-looping combustion. *Chem. Eng. Sci.* **2001**, *56* (10), 3101-3113.
(3) Ishida, M.; Jin, H. A Novel Chemical-Looping Combustor without NO_x Formation. *Ind. Eng. Chem. Res.* **1996**, *35* (7), 2469-2472.
(4) Kronberger, B.; Johansson, E.; Löffler, G.; Mattisson, T.; Lyngfelt, A.; Hofbauer, H. A Two-Compartment Fluidized Bed Reactor for CO_2 Capture by Chemical-Looping Combustion. *Chem. Eng. Technol.* **2004**, *27* (12), 1318-1326.
(5) Jerndal, E.; Mattisson, T.; Lyngfelt, A. Thermal Analysis of Chemical-Looping Combustion. *Chem. Eng. Res. Des.* **2006**, *84* (9), 795-806.
(6) Lyngfelt, A. Oxygen Carriers for Chemical Looping Combustion - 4000 h of Operational Experience. *Oil Gas Sci. Technol.* **2011**, *66* (2), 161-172
(7) Lyngfelt, A.; Mattisson, T. *Materials for chemical-looping combustion*; Efficient Carbon Capture for Coal Power Plants, Chapter 17, Ed. Stolten, D. and Sherer, V. ; WILEY-VCH Verlag GmbH & Co. KGaA: Weinheim, 2011.
(8) Hossain, M. M.; de Lasa, H. I. Chemical-looping combustion (CLC) for inherent CO_2 separations-a review. *Chem. Eng. Sci.* **2008**, *63* (18), 4433-4451.
(9) Adanez, J.; Abad, A.; Garcia-Labiano, F.; Gayan, P.; de Diego, L. F. Progress in Chemical-Looping Combustion and Reforming technologies. *Progr. Energy Combust. Sci.* **2012**, *38* (2), 215-282.
(10) Mattisson, T.; Lyngfelt, A.; Leion, H. Chemical-looping with oxygen uncoupling for combustion of solid fuels. *Int. J. Greenhouse Gas Control* **2009**, *3* (1), 11-19.
(11) Sarshar, Z.; Kleitz, F.; Kaliaguine, S. Novel oxygen carriers for chemical looping combustion: $La_{1-x}Ce_xBO_3$ (B = Co, Mn) perovskites synthesized by reactive grinding and nanocasting. *Energy & Environmental Science* **2011**, *4* (10), 4258-4269.
(12) Sarshar, Z.; Sun, Z.; Zhao, D.; Kaliaguine, S. Development of Sinter-Resistant Core–Shell $LaMn_xFe_{1-x}O_3$@$mSiO_2$ Oxygen Carriers for Chemical Looping Combustion. *Energy Fuels* **2012**, *26* (5), 3091-3102.
(13) Readman, J. E.; Olafsen, A.; Larring, Y.; Blom, R. $La_{0.8}Sr_{0.2}Co_{0.2}Fe_{0.8}O_{3-\delta}$ as a potential oxygen carrier in a chemical looping type reactor, an in-situ powder X-ray diffraction study. *J. Mater. Chem.* **2005**, *15* (19), 1931-1937.
(14) Leion, H.; Larring, Y.; Bakken, E.; Bredesen, R.; Mattisson, T.; Lyngfelt, A. Use of $CaMn_{0.875}Ti_{0.125}O_3$ as Oxygen Carrier in Chemical-Looping with Oxygen Uncoupling. *Energy Fuels* **2009**, *23* (10), 5276-5283.
(15) Rydén, M.; Lyngfelt, A.; Mattisson, T. $CaMn_{0.875}Ti_{0.125}O_3$ as oxygen carrier for chemical-looping combustion with oxygen uncoupling (CLOU)-Experiments in a continuously operating fluidized-bed reactor system. *Int. J. Greenhouse Gas Control* **2011**, *5* (2), 356-366.
(16) Rydén, M.; Lyngfelt, A.; Mattisson, T.; Chen, D.; Holmen, A.; Bjørgum, E. Novel oxygen-carrier materials for chemical-looping combustion and chemical-looping reforming;

$La_xSr_{1-x}Fe_yCo_{1-y}O_{3-\delta}$ perovskites and mixed-metal oxides of NiO, Fe_2O_3 and Mn_3O_4. *Int. J. Greenhouse Gas Control* **2008**, *2* (1), 21-36.
(17) Noorman, S.; Gallucci, F.; van Sint Annaland, M.; Kuipers, J. A. M. Experimental Investigation of Chemical-Looping Combustion in Packed Beds: A Parametric Study. *Ind. Eng. Chem. Res.* **2011**, *50* (4), 1968-1980.
(18) Rydén, M.; Leion, H.; Mattisson, T.; Lyngfelt, A., Combined oxides as oxygen carrier material for chemical-looping with oxygen uncoupling In *2nd International Conference on Chemical-Looping*, Darmstadt, 2012.
(19) Källen, M.; Rydén, M.; Dueso, C.; Mattisson, T.; Lyngfelt, A. $CaMn_{0.9}Mg_{0.1}O_{3-\delta}$ as Oxygen Carrier in a Gas-Fired 10 kW_{th} Chemical-Looping Combustion Unit. *submitted for publication* **2013**.
(20) Bakken, E.; Norby, T.; Stølen, S. Nonstoichiometry and reductive decomposition of $CaMnO_{3-\delta}$. *Solid State Ionics* **2005**, *176* (1–2), 217-223.
(21) Leonidova, E.; Leonidov, I. A.; Patrakeev, M. V.; Kozhevnikov, V. L. Oxygen non-stoichiometry, high-temperature properties, and phase diagram of $CaMnO_{3-\delta}$. *J. Solid State Electrochem.* **2011**, *15* (5), 1071-1075.
(22) Shulman, A.; Linderholm, C.; Mattisson, T.; Lyngfelt, A. High Reactivity and Mechanical Durability of $NiO/NiAl_2O_4$ and $NiO/NiAl_2O_4/MgAl_2O_4$ Oxygen Carrier Particles Used for more than 1000 h in a 10 kW CLC Reactor. *Ind. Eng. Chem. Res.* **2009**, *48* (15), 7400-7405.
(23) Linderholm, C.; Abad, A.; Mattisson, T.; Lyngfelt, A. 160 h of chemical-looping combustion in a 10 kW reactor system with a NiO-based oxygencarrier. *Int. J. Greenhouse Gas Control* **2008**, *2* (4), 520-530.
(24) Rørmark, L.; Wiik, K.; Stolen, S.; Grande, T. Oxygen stoichiometry and structural properties of $La_{1-x}A_xMnO_{3\pm\delta}$ (A = Ca or Sr and $0 \leq x \leq 1$). *J. Mater. Chem.* **2002**, *12* (4), 1058-1067.
(25) Ksepko, E.; Figa, J.; Talik, E. Preparation and Characterization of $Sr(Mn_{1-x}Ni_x)O_3$ Solid Solution in Relation to Their Use in Chemical Looping Oxygen Transfer. *5th Annual International Pittsburgh Coal Conference, Pittsburgh, PA, USA* **2008**.
(26) Rasband, W. S. *ImageJ*, National Institutes of Health: Bethesda, 1997.
(27) Rydén, M.; Moldenhauer, P.; Lindqvist, S.; Mattisson, M.; Lyngfelt, A. Measuring attrition resistance of oxygen carrier particles for chemical-looping combustion with the jet cup method. *Submitted for publication* **2012**.
(28) Kunii, D.; Levenspiel, O. *Fluidization Engineering*; Butterworth-Heinemann: Boston, 1991.
(29) Arjmand, M.; Keller, M.; Leion, H.; Mattisson, T.; Lyngfelt, A. Oxygen Release and Oxidation Rates of $MgAl_2O_4$-Supported CuO Oxygen Carrier for Chemical-Looping Combustion with Oxygen Uncoupling (CLOU). *Energy Fuels* **2012**, *26* (11), 6528-6539.
(30) Siriwardane, R.; Tian, H.; Miller, D.; Richards, G.; Simonyi, T.; Poston, J. Evaluation of reaction mechanism of coal–metal oxide interactions in chemical-looping combustion. *Combust. Flame* **2010**, *157* (11), 2198-2208.
(31) Varela, A.; Dios, S. d.; Parras, M.; Hernando, M. a.; Fernández-Díaz, M. T.; Landa-Cánovas, A. R.; González-Calbet, J. M. Ordered Rock-Salt Related Nanoclusters in $CaMnO_2$. *J. Am. Chem. Soc.* **2009**, *131* (24), 8660-8668.
(32) Reller, A.; Davoodabady, G.; Oswald, H. R. Reversible topotactic reduction of perovskite-related calcium manganese oxides. *Thermochim. Acta* **1985**, *83* (1), 121-124.
(33) Poeppelmeier, K. R.; Horowitz, H. S.; Longo, J. M. Oxide solid solutions derived from homogeneous carbonate precursors: The CaO-MnO solid solution. *Journal of the Less Common Metals* **1986**, *116* (1), 219-227.

Tables

Table 1 Physical characteristics of the fresh oxygen carriers investigated in this work.

Sample	System.	Crushing strength [N]	Bulk density [g/cm^3]	BET specific surface area [m^2/g]
CM	$CaMnO_{3-\delta}$	1.4	1.62	0.28
CLM	$Ca_{0.9}La_{0.1}MnO_{3-\delta}$	1.2	1.72	0.44
CLMM	$Ca_{0.9}La_{0.1}Mn_{0.9}Mg_{0.1}O_{3-\delta}$	1.3	2.27	0.48
CLMT	$Ca_{0.9}La_{0.1}Mn_{0.9}Ti_{0.1}O_{3-\delta}$	1.5	1.68	0.40
CLMF	$Ca_{0.9}La_{0.1}Mn_{0.9}Fe_{0.1}O_{3-\delta}$	2.8	2.21	0.23
CLMC	$Ca_{0.9}La_{0.1}Mn_{0.9}Cu_{0.1}O_{3-\delta}$	1.7	3.08	0.08

Table 2 Analysis of the as-received and devolatilized Swedish wood char used as fuel in this work.

	Ultimate [wt.%] (dry basis)				
	Ash	N	C	H	S
As received	9.7	0.51	78.7	2.9	0.02
After devolatilization	14.3	0.71	88.9	<0.3	0.01

Table 3 Oxygen concentrations at 900 and 1000^{o}C after 360 s of inert gas purge before and after the fuel cycles at 950^{o}C.

Sample	O_2 concentration at 900°C [%]		O_2 concentration at 1000°C [%]	
	before fuel	after fuel	before fuel	after fuel
CM	0.59	0.59	0.96	0.89
CLM	0.30	0.25	0.77	0.72
CLMM	0.36	0.33	0.69	0.56
CLMT	0.22	0.21	0.61	0.57
CLMF	0.35	0.34	0.87	0.82
CLMC	0.78	Defluidized	1.06	Defluidized

Table 4 Physical characteristics of the oxygen carriers after the reactivity test.

Sample	Bulk density [g/cm^3]	BET specific surface area [m^2/g]
CM	0.89	0.36
CLM	1.21	0.40
CLMM	1.27	0.45
CLMT	1.26	0.40
CLMF	1.48	0.25

Figures

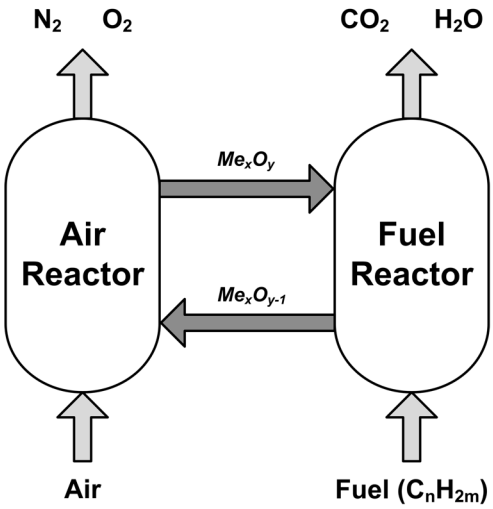

Figure 1 Schematic of the chemical-looping combustion (CLC) process.

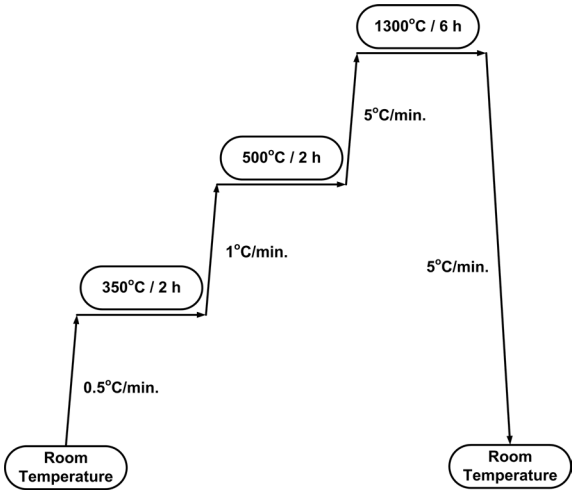

Figure 2 Temperature-time schedules for the processing of carrier extrudates.

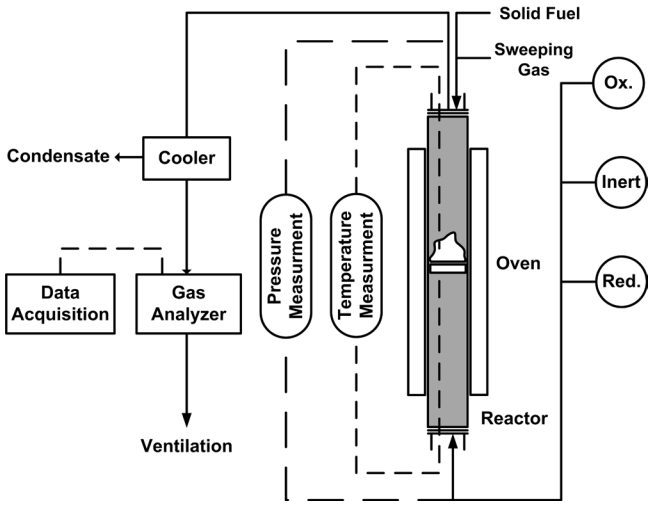

Figure 3 Experimental setup used in this investigation.

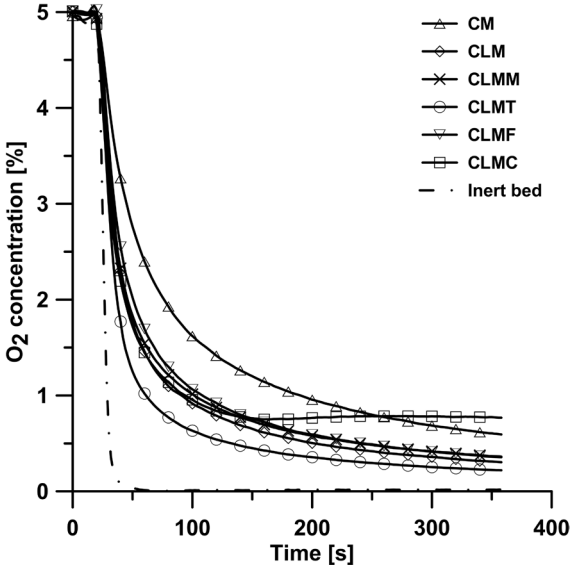

Figure 4 Oxygen release profiles for various carriers investigated in this work during inert gas purge for 360 s at 900^{o}C.

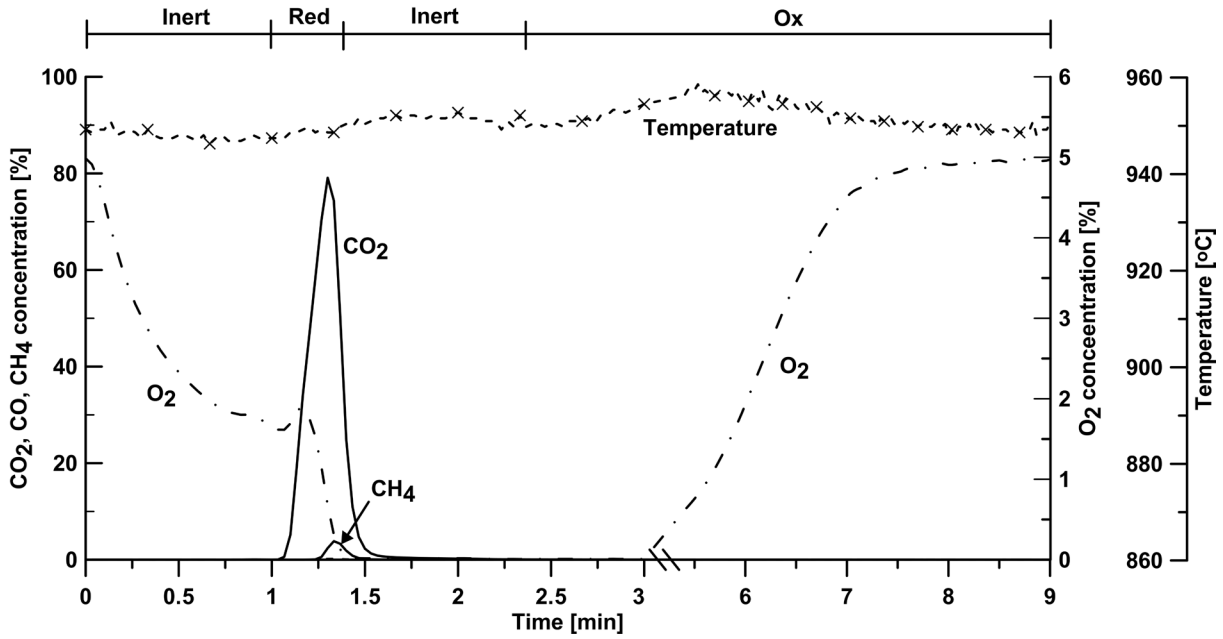

Figure 5 Concentration of various gaseous species during conversion of CH_4 at 950°C for 20 s using CLMF (15 g sample) followed by oxidation in 5%O_2; the temperature profile during reduction and oxidation periods is also shown.

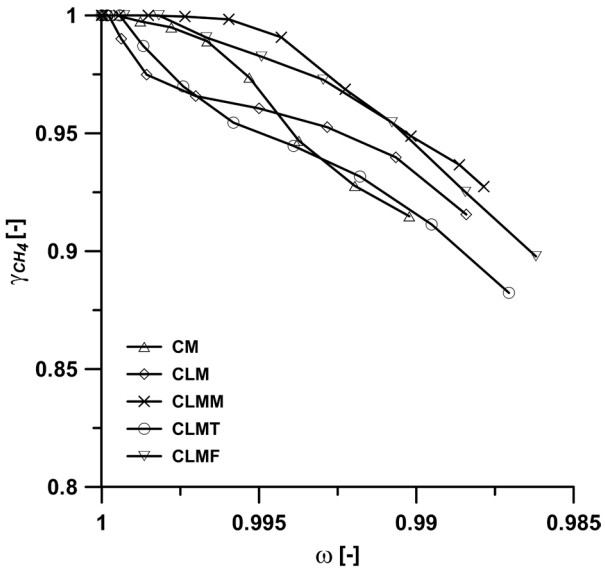

Figure 6 Variation of gas yield, γ_{CH_4}, with mass-based conversion, ω, for different oxygen carriers during conversion of CH_4 for 20 s at 950°C.

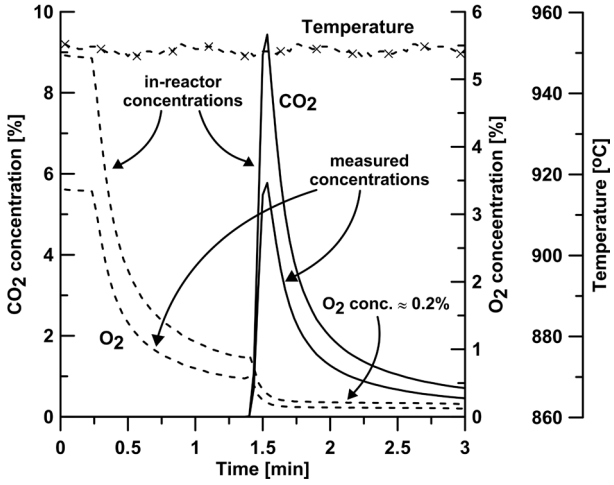

Figure 7 Concentration of various gaseous species during conversion of 0.1 g of devolatilized wood char at 950°C using CM (5 g sample in 10 g quartz); the temperature profile during fuel reduction is also shown.

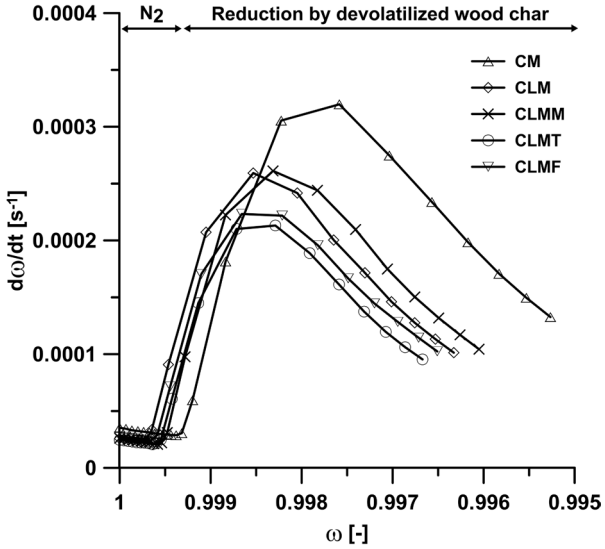

Figure 8 Variation of mass-based conversion derivative, $\frac{d\omega}{dt}$, with mass-based conversion, ω, of the perovskite carriers during conversion of 0.1 g of devolatilized wood char at 950°C (5 g sample in 10 g quartz) at 950°C.

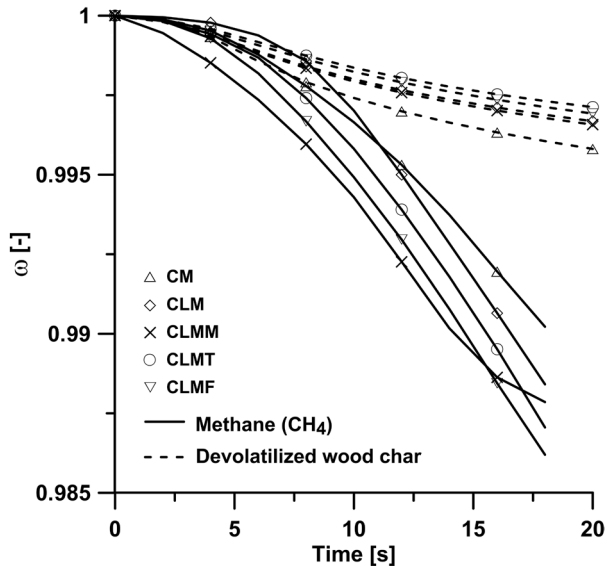

Figure 9 Variation of mass-based conversion, ω, of the oxygen carriers with time for reduction with methane and 0.1 g of devolatilized wood char at 950°C.

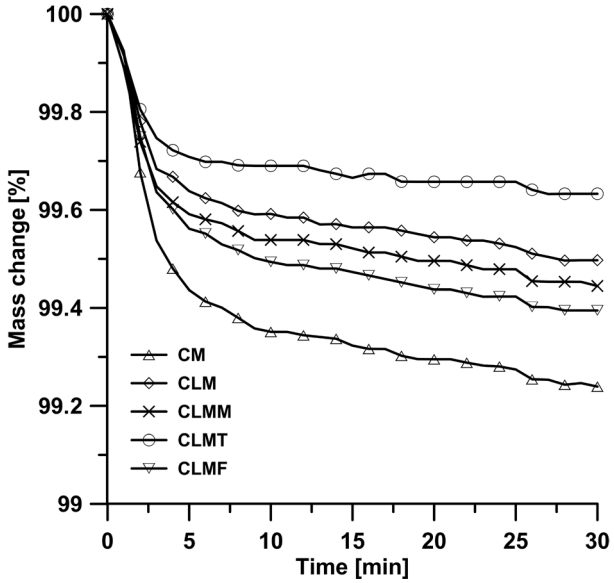

Figure 10 Oxygen capacity (R_O) of the carriers investigated in this work during cycling between air (20.8% O_2) and high purity inert gas (N_2) at 950°C in a thermogravimetric analyzer.

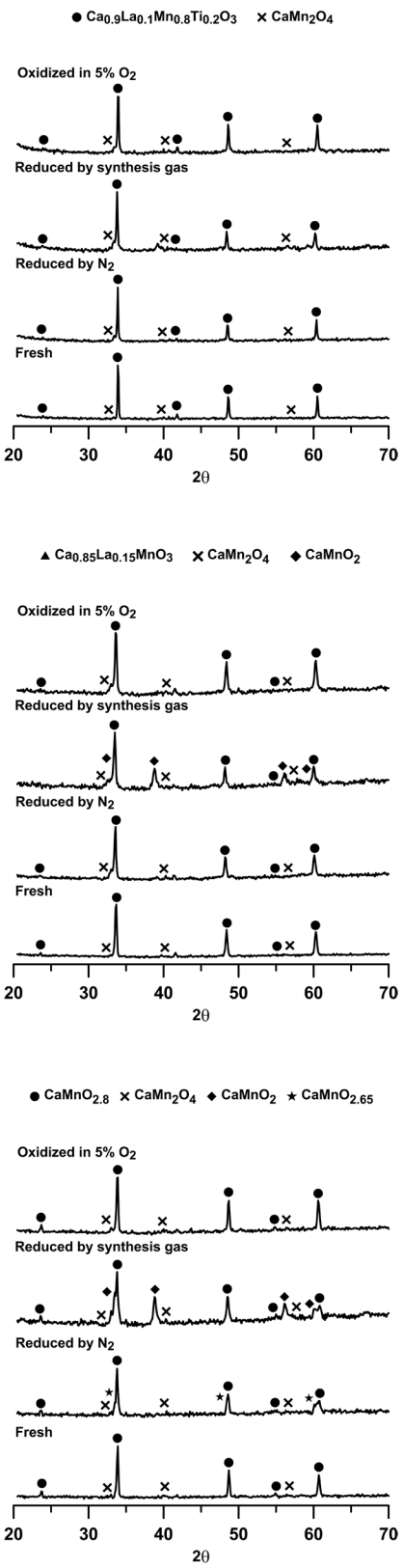

Figure 11 Comparative XRD signatures of fresh, reduced in N_2, reduced by synthesis gas and oxidized (5% O_2 in N_2) at 950°C: (bottom) CM (middle) CLM and (top) CLMT.

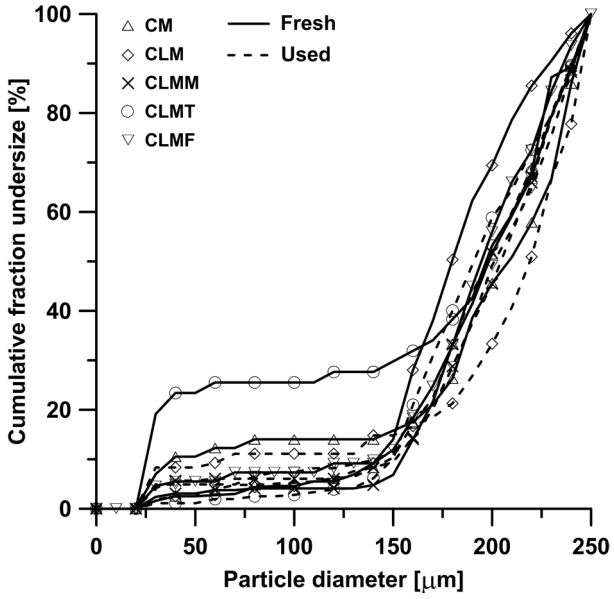

Figure 12 Particle size distributions (PSD) of the fresh and used oxygen carriers.

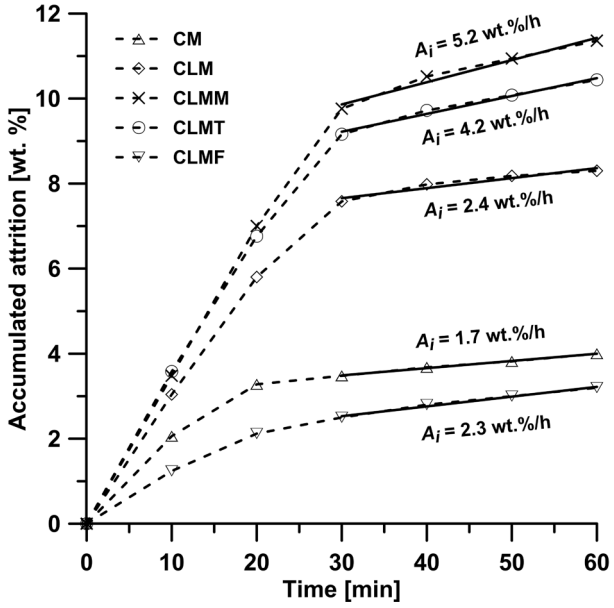

Figure 13 Attrition rates of the used oxygen carrier particles.

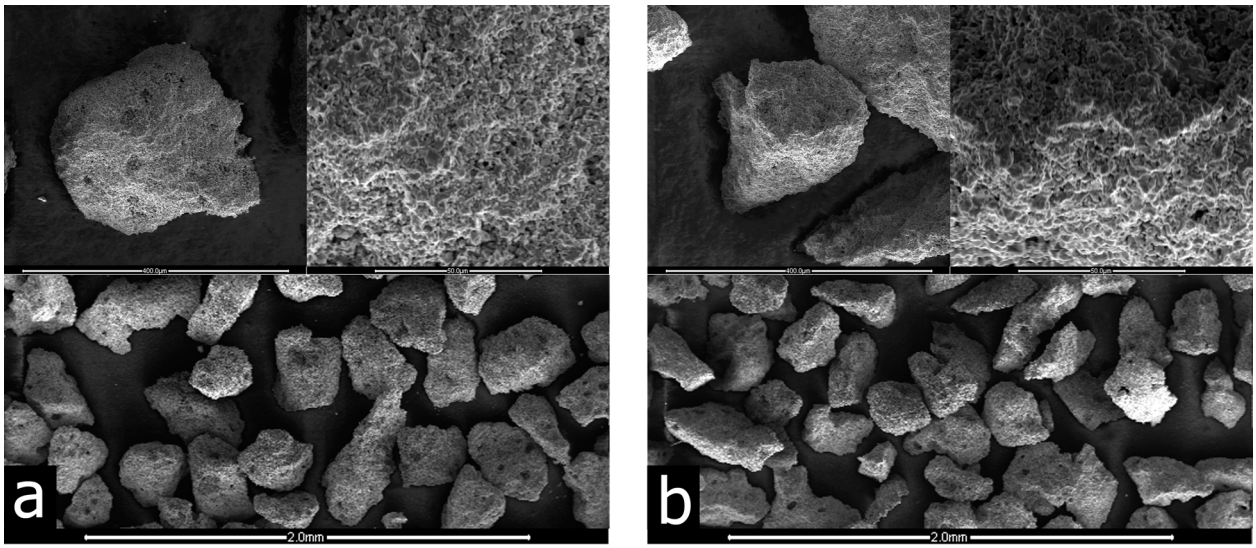

Figure 14 ESEM images of (a) fresh and (b) used CLM particles after the reactivity tests. The size bars for the top images are 400 and 50 µm while those of the bottom images are 2 mm.